

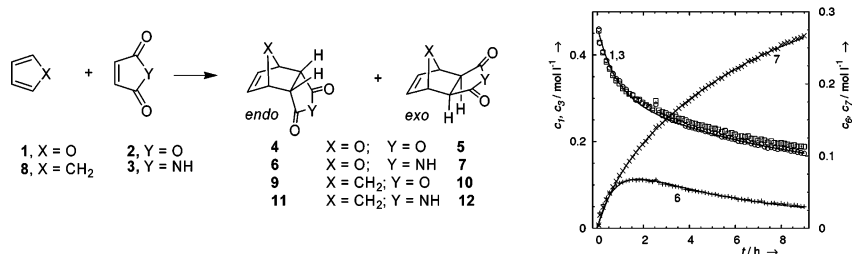
An Experimental and Theoretical Study of Stereoselectivity of Furan–Maleic Anhydride and Furan–Maleimide Diels–Alder Reactions

Lubomír Rulíšek,[†] Pavel Šebek,[‡] Zdeněk Havlas,[†] Richard Hrabal,[§] Pavel Čapek,^{||} and Aleš Svatoš^{*,‡}

Max-Planck-Institute for Chemical Ecology, Hans-Knöll-Str. 8, 07745, Jena, Germany, Institute of Organic Chemistry and Biochemistry and Center for Complex Molecular Systems and Biomolecules, Academy of Sciences of the Czech Republic Flemingovo náměstí 2, 166 10 Prague 6, Czech Republic, and Laboratory of NMR Spectroscopy and Department of Organic Technology, Prague Institute of Chemical Technology, Technická 5, Prague 6, Zentiva a.s., U Kabelovny 130, Prague 10, Czech Republic

svatos@ice.mpg.de

Received April 15, 2005



The stereoselectivity of the reaction of furan (1) with maleic anhydride (2) and maleimide (3) was studied experimentally and theoretically. Although the two reactions are highly similar with regard to their preference for *endo* and *exo* stereoisomers, notable differences were experimentally observed and explained on the basis of calculated reaction-free energies and transition-state barriers. The experimental values of rate constants ($k_{1+2endo} = (1.75 \pm 0.48) \times 10^{-5}$; $\text{mol}^{-1} \text{l s}^{-1}$; $k_{1+2exo} = (3.10 \pm 0.55) \times 10^{-5}$; $\text{mol}^{-1} \text{l s}^{-1}$; $k_{1+3endo} = (1.93 \pm 0.082) \times 10^{-5}$; $\text{mol}^{-1} \text{l s}^{-1}$; $k_{1+3exo} = (1.38 \pm 0.055) \times 10^{-5}$; $\text{mol}^{-1} \text{l s}^{-1}$ all at 300 K) and the observed reaction course clearly confirm that neither of these reactions are prototypical examples of Diels–Alder [4 + 2] cycloadditions, whose dominant preference is for *endo* isomers. However, only by comparing their energetics—calculated at the CCSD(T) level of theory—with the analogous reactions involving cyclopentadiene (8) as a diene can these observations be understood. The low thermodynamic stability of furan [4 + 2] adducts opens retro-Diels–Alder reaction channels and overrules the very small kinetic preference (calculated and measured here) of initial formation for *endo* stereoisomers. On a macroscopic scale “an irregular”—thermodynamically more stable—*exo* stereoisomer was consequently observed as a dominant species.

1. Introduction

For many years, Diels–Alder reactions have attracted the interest of both experimental and theoretical chemists.^{1–5} Extensive efforts have been made to understand their reaction mechanism (concerted versus stepwise,

synchronous versus asynchronous)^{6–8} and the factors determining *endo/exo* stereoselectivity.^{9–12} While experi-

* Corresponding author. Tel (Fax): +49-3641-571700(01).

[†] Institute of Organic Chemistry and Biochemistry AS CR.

[‡] Zentiva, a.s.

[§] Laboratory of NMR spectroscopy, Prague Institute of Technology.

^{||} Department of Organic Chemistry, Prague Institute of Technology.

[‡] Max-Planck-Institute for Chemical Ecology.

(1) Hoffmann, R.; Woodward, R. B. *J. Am. Chem. Soc.* **1965**, *87*, 4388.

(2) Sauer, J.; Sustmann, R. *Angew. Chem., Int. Ed. Engl.* **1980**, *19*, 779.

(3) Stephenson, L. M.; Smith, D. E.; Current, S. P. *J. Org. Chem.* **1982**, *47*, 4710.

(4) Robertson, A.; Philp, D.; Spencer, N. *Tetrahedron* **1999**, *55*, 11365.

(5) Manka, J. T.; Douglass, A. G.; Kaszynski, P.; Friedli, A. C. *J. Org. Chem.* **2000**, *65*, 5202.

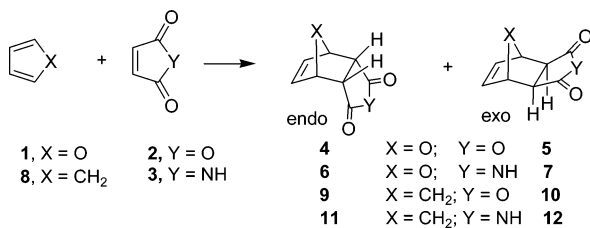
(6) Houk, K. N.; Li, Y.; Evanscek, J. D. *Angew. Chem., Int. Ed. Engl.* **1992**, *31*, 682.

(7) Goldstein, E.; Beno, B.; Houk, K. N. *J. Am. Chem. Soc.* **1996**, *118*, 6036.

(8) Chen, J. S.; Houk, K. N.; Foote, C. S. *J. Am. Chem. Soc.* **1998**, *120*, 12303.

(9) Sbai, A.; Branchadell, V.; Oliva, A. *J. Org. Chem.* **1996**, *61*, 621.

(10) Domingo, L. R.; Picher, M. T.; Andres, J.; Safont, V. S. *J. Org. Chem.* **1997**, *62*, 1775.

SCHEME 1. Overview of Diels–Alder [4 + 2] Cycloadditions Studied in This Work


mental measurements can provide accurate rate constants for the different reaction pathways, high-level quantum chemical calculations are often necessary to explain the observed phenomena at the electronic level, predict the substituent effects, and evaluate sterical interactions between the participating species. In recent years, the advances in the methodology of quantum-chemical calculations (e.g., the development of new DFT functionals, continuum solvation models) and the growth of computational power have provided the accuracy needed to quantitatively explain experimental observations. In conjunction with convenient methods for the analysis of correlated wave functions (e.g., natural bond orbital analysis (NBO),¹³ Bader's atoms-in-molecules theory¹⁴), in theoretical organic chemistry many well-established principles of the theory of molecular orbitals applied to cycloaddition reactions (e.g., secondary orbital interactions, SOI) are undergoing a thorough reevaluation.^{15,16}

In this work, we focus our attention on two [4 + 2] cycloadditions, in which furan **1** reacts with maleic anhydride **2** or maleimide **3** to provide a mixture of *endo/exo* isomers of the corresponding adducts (Scheme 1).

The former reaction (**1** + **2**) was studied both experimentally^{17–19} and theoretically.^{20,21,22} Nevertheless, recent NMR measurements,^{23,24} supported by correlated quantum chemical calculations, sharply disagree with the earlier results of Lee and Herndon.¹⁹ The new results suggest that the predominant formation of **5** is caused by its higher thermodynamic stability, and only a very small kinetic preference for isomer **4** (the activation barrier is about 0.8 kJ mol⁻¹ higher²² for isomer **5**) was determined. The situation is even more complicated for the latter reaction, which involves maleimide (**1** + **3**).

(11) Di Valentin, C.; Freccero, M.; Sarzi-Amade, M.; Zanaletti, R. *Tetrahedron* **2000**, *56*, 2547.

(12) Yoshitake, Y.; Nakagawa, H.; Eto, M.; Harano, K. *Tetrahedron Lett.* **2000**, *41*, 4395.

(13) Reed, A. E.; Curtiss, L. A.; Weinhold, F. *Chem. Rev.* **1988**, *88*, 899.

(14) Bader, R. W. F. *Acc. Chem. Res.* **1985**, *18*, 9.

(15) García, J. I.; Mayoral, J. A.; Salvatella, L. *Acc. Chem. Res.* **2000**, *33*, 658.

(16) Arrieta, A.; Cossio, F. P.; Lecea, B. *J. Org. Chem.* **2001**, *66*, 6178.

(17) Woodward, R. B.; Baer, H. *J. Am. Chem. Soc.* **1948**, *70*, 1161.

(18) Anet, F. A. L. *Tetrahedron Lett.* **1962**, 1219.

(19) Lee, M. W.; Herndon, W. C. *J. Org. Chem.* **1978**, *43*, 516.

(20) Dewar, M. J. S.; Pierini, A. B. *J. Am. Chem. Soc.* **1984**, *106*, 203.

(21) Kappe, C. O.; Murphree, S. S.; Padwa, A. *Tetrahedron* **1997**, *53*, 14179.

(22) Calvo-Losada, S.; Suárez, D. *J. Am. Chem. Soc.* **2000**, *122*, 390.

(23) Zhulin, V. M.; Bogdanov, V. S.; Keltseva, M. V.; Kabotyanskaya, E. B.; Koreshov, Y. D. *Bull. Acad. Sci. USSR D. Chem. Sci.* **1989**, *38*, 2303.

(24) Zhulin, V. M.; Keltseva, M. V.; Bogdanov, V. S.; Koreshov, Y. D.; Kabotyanskaya, E. B. *Bull. Acad. Sci. USSR D. Chem. Sci.* **1990**, *39*, 456.

This reaction, originally reported²⁵ to provide at room temperature the *endo*-adduct **6**, was reexamined by Berson and Swidler.²⁶ The preferential formation of **6** was found to be an oversight. The reaction provides a mixture of **6** and **7** in differing proportions depending on conditions; however, a detailed study of the reaction kinetics and its theoretical interpretation has not yet been performed. On the contrary, in the closely related reaction of cyclopentadiene (**8**) with dienophiles **2** and **3**, the obtained Diels–Alder adducts are predominantly *endo*-isomers **9**²⁷ and **11**,²⁸ respectively.

The objective of this work is to explain the origin of the observed reaction kinetics and *endo/exo* stereoselectivity of the title Diels–Alder reactions. To achieve this goal, the reaction of **1** with **2** and both with **3** and the thermal stability and/or isomerization of pure adducts **6** and **7** were studied at different temperatures using ¹H NMR spectrometry. The obtained data were fitted to relevant plausible kinetic models and the corresponding rate constants calculated. To reproduce the experimental results and to analyze the observed trends using the decomposition of electronic wave functions, a series of quantum chemical calculations were performed for both reaction channels of the two title reactions and the corresponding reactions of both dienophiles with cyclopentadiene (**8**) (as the examples of prototypical Diels–Alder [4 + 2] cycloadditions).

2. Experimental Methods

Chemicals. Chemicals were obtained from commercial sources; furan, maleic anhydride, maleimide, and 7-oxabicyclo[2.2.1]heptene-*exo*-2,3-dicarboxylic anhydride (**5**) and used as purchased. A sample of 7-oxabicyclo[2.2.1]heptene-*endo*-2,3-dicarboxylic imide (**6**) was prepared in our laboratory according to modified a procedure adopted from ref 26, and a sample of 7-oxabicyclo[2.2.1]heptene-*exo*-2,3-dicarboxylic imide (**7**) was prepared from anhydride **4**.

¹H NMR Measurements and Estimation of Kinetic Constants. All kinetic experiments were performed directly in NMR tubes under argon atmosphere in screw-cap tubes and at a constant temperature (300 and 338 K, respectively). Acetonitrile-*d*₃, CD₃CN, was used as the solvent in all the cases. Before the start of each run, a known amount of **2** or **3** was dissolved in 0.5 mL of acetonitrile-*d*₃ in a screw-cap NMR tube, and a constant volume of furan was injected via septum. A series of ¹H NMR (400.13 MHz) spectra were recorded. Data for the first experiment were collected regularly after 2 min of lag time. The time delay between the following experiments within a series was, for the reaction between **1** and **2**, 2 min for the first 9 points and 10 min for an additional 11 points, and an additional 30 points were collected every 60 min; for the reaction of **1** with **3**, 5 min for the first 10 points and 30 min for an additional 20 points. Chemical shifts in ppm were referenced to tetramethylsilane (TMS). Data were acquired to 8192 data points and processed to 16 384 data points by zero-filling. Prior to a Fourier transformation, FIDs were multiplied by the exponential function (LB = 0.2 Hz). Each experiment was baseline-corrected, and the signals were integrated. The integrals were referenced with respect to the whole integral of all signals within the spectrum. Isomerization experiments of **6** and **7** were performed in a similar fashion.

(25) Kwart, H.; Burchuk, I. *J. Am. Chem. Soc.* **1952**, *74*, 3094.

(26) Berson, J.; Swidler, R. *J. Am. Chem. Soc.* **1954**, *76*, 4060.

(27) Diels, O.; Alder, K. *Justus Liebigs Ann. Chem.* **1928**, *460*, 111.

(28) Harvey, S. C. *J. Am. Chem. Soc.* **1949**, *71*, 1121.

Initial molar concentrations were determined from the known volumes of reactants provided that the mixing was ideal (i.e., no volume contraction or expansion was assumed). The obtained data were used for a detailed analysis of the kinetic of the both reactions using Bayesian fits for a constructed kinetic model.^{29,30} To estimate parameters, the time dependences of the molar concentrations of isomers were included only in the objective function because of the linear dependence of the responses of reactants.

Computational Details. The calculations were performed with MOLPRO^{31,32} (coupled cluster–CCSD(T)–single point energies) and Gaussian 98³³ (all the remaining calculations) programs. Three basis sets were used throughout the calculations: 6-31+G(d),³⁴ 6-311++G(2p,d),³⁵ and aug-cc-pVDZ.³⁶ The optimization of molecular geometries was carried out at the B3LYP/6-31+G(d) and MP2/6-31+G(d) levels. The single-point electronic energies were computed at the CCSD(T)/aug-cc-pVDZ level, using MP2/6-31+G(d) optimized geometries. Vibrational analyses were carried out at the B3LYP/6-31+G(d) level and the computed frequencies used for the subsequent thermochemistry calculations, using the standard formulas of statistical thermodynamics in the ideal gas approximation. In this way, ΔG_{gas} values were obtained for each adduct and transition state. Solvation Gibbs energies, ΔG_{solv} , for all species concerned have been computed in the framework of the PCM reaction field model of Tomasi and co-workers.^{37,38} The standard dielectric constants for three solvents were used: (ϵ_r (H₂O) = 78.39, ϵ_r (CH₃CN) = 36.64, ϵ_r (benzene) = 2.247).

3. Results and Discussion

3.1. Kinetic Experiments. Model Development.

The first system comprised **1**, **2**, **4**, and **5**; the second system, **1**, **3**, **6**, and **7**. To formulate a model more easily, reaction components were denoted in agreement with Scheme 1 as A_x where x stands for the compound numbers.

Acetonitrile- d_3 did not react under conditions used in this work and thus does not appear in the list of components involved in mass balance considerations. We assumed that three reversible reactions were possible

among all four components involved in the first reaction system



as well as among all the components involved in the second reaction system:



For the first reaction system, rates of reaction steps, r_j , were defined as

$$r_{\text{I}} = k_{\text{I}}^{\text{f}}c_1c_2 - k_{\text{I}}^{\text{b}}c_4 \quad (7)$$

$$r_{\text{II}} = k_{\text{II}}^{\text{f}}c_1c_2 - k_{\text{II}}^{\text{b}}c_5 \quad (8)$$

$$r_{\text{III}} = k_{\text{III}}^{\text{f}}c_4 - k_{\text{III}}^{\text{b}}c_5 \quad (9)$$

provided that these reaction steps are elementary. Molar concentrations of individual components A_1 – A_7 are denoted c_i , and rate constants (kinetic parameters) are denoted k_i^{f} and k_i^{b} for forward and backward steps, respectively. Similar equations for the rates of elementary steps, r_{IV} , r_{V} , and r_{VI} were derived for the second system characterized by rate constants of $k_{\text{IV–VI}}^{\text{f}}$ and $k_{\text{IV–VI}}^{\text{b}}$.

Kinetics. Reaction mechanisms proposed for both reaction systems consisted of three reversible elementary reaction steps. To elucidate the role of direct conversion of *endo*-adduct to *exo*-adduct (reaction steps III and VI) in the reaction mechanism, several preliminary kinetic experiments were performed. Specifically, we focused on the conversion of the thermodynamically less stable **4** and **6** to the thermodynamically more stable **5** and **7** isomers.

After injecting a known amount of **6** into the NMR tube with CD₃CN, we observed a time lag in the increase of the concentration of **7**; see Figure 1. Similar time lags were found for other temperatures as well as for the decomposition of **4**. The absence of the direct conversion of the *endo*- to *exo*-adduct is strongly supported by the results of the quantum-chemical calculations. The direct conversion barrier (reaction steps III and VI) was found to be significantly larger than the energy barrier of the *endo/exo*-adduct formation and/or decomposition. (In fact, the estimate of a barrier height of more than 220 kJ/mol was made from the linearly interpolated structure of *endo/exo* adducts, whose geometry optimization has ended up in its dissociation into the reactants, i.e., in one of the transition states reported throughout this paper. This fact makes the definition of a barrier height for the direct conversion physically unsound.) We recognized these facts to be sufficient for excluding the reaction steps (III) and (VI) from the next data treatment and discussion, i.e., $k_{\text{III}}^{\text{f}} = k_{\text{VI}}^{\text{b}} = k_{\text{VI}}^{\text{f}} = k_{\text{III}}^{\text{b}} = 0$. This contradicts the conclusions of Zhulin et al.,³⁹ who found the irreversible

(29) Stewart, W. E.; Caracotsios, M.; Sorensen, J. P. *AIChE J.* **1992**, *38*, 641.

(30) Hunter, W. G. *Ind. Eng. Chem. Fundam.* **1967**, *5*, 461.

(31) MOLPRO is a package of ab initio programs written by Werner, H.-J. and Knowles, P. J. with contributions from Amos, R. D.; Bernhardsson, A.; Berning, A.; Celani, P.; Cooper, D. L.; Deegan, M. J. O.; Dobbyn, A. J.; Eckert, F.; Hampel, C.; Hetzer, G.; Korona, T.; Lindh, R.; Lloyd, A. W.; McNicholas, S. J.; Manby, F. R.; Meyer, W.; Mura, M. E.; Nicklass, A.; Palmieri, P.; Pitzer, R.; Rauhut, G.; Schütz, M.; Stoll, H.; Stone, A. J.; Tarroni, R.; Thorsteinsson, T.

(32) Hampel, C.; Peterson, K.; Werner, H.-J. *Chem. Phys. Lett.* **1992**, *190*, 1.

(33) Gaussian 98, Revision A.7: Frisch, M. J.; Trucks, G. W.; Schlegel, H. B.; Scuseria, G. E.; Robb, M. A.; Cheeseman, J. R.; Zakrzewski, V. G.; Montgomery, J. A., Jr.; Stratmann, R. E.; Burant, J. C.; Dapprich, S.; Millam, J. M.; Daniels, A. D.; Kudin, K. N.; Strain, M. C.; Farkas, O.; Tomasi, J.; Barone, V.; Cossi, M.; Cammi, R.; Mennucci, B.; Pomelli, C.; Adamo, C.; Clifford, S.; Ochterski, J.; Petersson, G. A.; Ayala, P. Y.; Cui, Q.; Morokuma, K.; Malick, D. K.; Rabuck, A. D.; Raghavachari, K.; Foresman, J. B.; Cioslowski, J.; Ortiz, J. V.; Stefanov, B. B.; Liu, G.; Liashenko, A.; Piskorz, P.; Komaromi, I.; Gomperts, R.; Martin, R. L.; Fox, D. J.; Keith, T.; Allaham, M. A.; Peng, C. Y.; Nanayakkara, A.; Gonzalez, C.; Challacombe, M.; Gill, P. M. W.; Johnson, B.; Chen, W.; Wong, M. W.; Andres, J. L.; Gonzalez, C.; HeadGordon, M.; Replogle, E. S.; Pople, J. A. Gaussian, Inc., Pittsburgh, PA, 1998.

(34) Hehre, W. J.; Ditchfield, R.; Pople, J. A. *J. Chem. Phys.* **1972**, *56*, 2257.

(35) Krishnan, R.; Binkley, J. S.; Seeger, R.; Pople, J. A. *J. Chem. Phys.* **1980**, *72*, 650.

(36) Woon, D. E.; Dunning, T. H., Jr. *J. Chem. Phys.* **1993**, *98*, 1358.

(37) Miertus, S.; Scrocco, E.; Tomasi, J. *Chem. Phys.* **1981**, *55*, 117.

(38) Cossi, M.; Barone, V.; Cammi, R.; Tomasi, J. *Chem. Phys. Lett.* **1996**, *255*, 327.

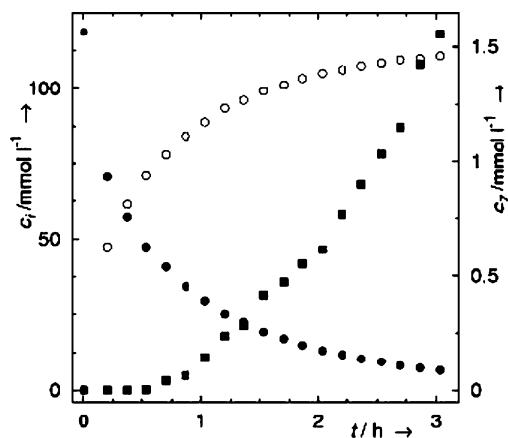


FIGURE 1. The time dependences of the molar concentrations of **1** (○), **6** (●), and **7** (■) for decomposition of **6** at 338 K. The concentration of **3** was omitted for the sake of clarity.

TABLE 1. Rate Constants for [4 + 2] Reaction of Furan (**1**) and Maleic Anhydride (**2**) at 300 K

parameter	dimension	point estimate	interval estimate ^a
$k_{\text{IV}}^{\text{f}}(\text{endo})$	$\text{mol}^{-1} \text{l s}^{-1}$	1.75×10^{-5}	$\pm 4.8 \times 10^{-6}$
$k_{\text{IV}}^{\text{b}}(\text{endo})$	s^{-1}	1.38×10^{-4}	$\pm 3.0 \times 10^{-7}$
$k_{\text{II}}^{\text{f}}(\text{exo})$	$\text{mol}^{-1} \text{l s}^{-1}$	3.10×10^{-5}	$\pm 5.5 \times 10^{-6}$
$k_{\text{II}}^{\text{b}}(\text{exo})$	s^{-1}	~ 0	

^a Joint confidence limits for the probability level of 0.9545.

TABLE 2. Rate Constants for [4 + 2] Reaction of Furan (**1**) and Maleimide (**3**) at 300 K

parameter	dimension	point estimate	interval estimate ^a
$k_{\text{IV}}^{\text{f}}(\text{endo})$	$\text{mol}^{-1} \text{l s}^{-1}$	1.93×10^{-5}	$\pm 8.2 \times 10^{-7}$
$k_{\text{IV}}^{\text{b}}(\text{endo})$	s^{-1}	5.48×10^{-6}	$\pm 4.5 \times 10^{-6}$
$k_{\text{IV}}^{\text{f}}(\text{exo})$	$\text{mol}^{-1} \text{l s}^{-1}$	1.38×10^{-5}	$\pm 5.5 \times 10^{-7}$
$k_{\text{IV}}^{\text{b}}(\text{exo})$	s^{-1}	3.2×10^{-7}	$\pm 1.7 \times 10^{-7}$

^a Joint confidence limits for the probability level of 0.9545.

TABLE 3. Rate Constants for [4 + 2] Reaction of Furan (**1**) and Maleimide (**3**) at 338 K

parameter	dimension	point estimate	interval estimate ^a
$k_{\text{IV}}^{\text{f}}(\text{endo})$	$\text{mol}^{-1} \text{l s}^{-1}$	1.67×10^{-4}	$\pm 1.7 \times 10^{-5}$
$k_{\text{IV}}^{\text{b}}(\text{endo})$	s^{-1}	2.05×10^{-4}	$\pm 2.2 \times 10^{-5}$
$k_{\text{IV}}^{\text{f}}(\text{exo})$	$\text{mol}^{-1} \text{l s}^{-1}$	1.37×10^{-4}	$\pm 4.2 \times 10^{-6}$
$k_{\text{IV}}^{\text{b}}(\text{exo})$	s^{-1}	3.32×10^{-6}	$\pm 1.7 \times 10^{-6}$

^a Joint confidence limits for the probability level of 0.9545.

conversion of **4** to **5** to be significant to explain their kinetic data.

The Diels–Alder reactions yielding isomers **4**–**7** with varying initial concentrations of the corresponding reactants and the kinetic measurements were repeated twice to get more reliable data sets. The rate constants determined for both reaction systems are summarized in Tables 1–3. In addition to the point estimates, we have also determined their interval estimates (joint confidence limits) so as to assess the significance of the reaction mechanisms and the corresponding individual rate constants. The higher the joint confidence limit with regard

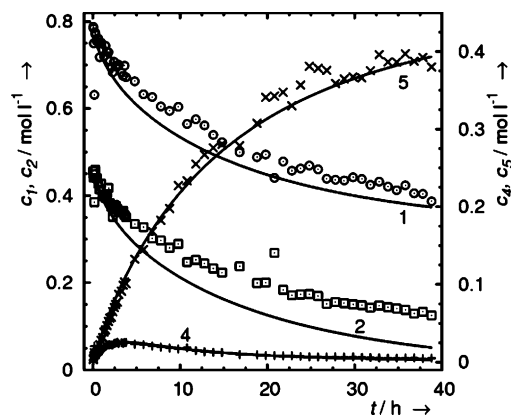


FIGURE 2. Comparison of experimental and predicted responses for reaction of **1** and **2** at 300 K. Experimental points: **1** (○), **2** (□), **4** (+), **5** (×).

to the point estimate, the less reliable the point estimate (or, rate constant) is.

The kinetic measurements also confirmed the higher thermodynamic stability of the *exo*-adduct; the ratio of the forward and backward rate constants of the formation of the *exo*-adduct was much higher than the formation of the *endo*-isomers. This phenomenon is more significant for the first reaction system of anhydride **2**. In this case the formation of **5** at a temperature of 300 K was almost irreversible, as indicated by the negligible value of k_{II}^{b} (Table 1). Apart from temperature, the forward rate constant of the formation of **6**, i.e., k_{IV}^{f} , was higher than the corresponding rate constant of the formation of **7** (k_{V}^{f}).

However, the kinetically favored formation of **5** was called into question by Lee and Herndon,¹⁹ who found the initial rate of formation of **4** to be 456 times larger than that of **5**. In contrast, our results for the first reaction system support the conclusions of Anet,¹⁸ who observed that the ratio between the *exo/endo*-adducts was close to two (in favor of *exo*). The absolute values of the rate constants reported by Lee and Herndon¹⁹ cannot be directly compared to our data, since they performed the experiments at 313 K. The only rate constant that can be approximately compared to the data from the literature¹⁹ ($1.6 \times 10^{-5} \text{ mol}^{-1} \text{ l s}^{-1}$) is k_{II}^{f} (300 K) = $3.10 \times 10^{-5} \text{ mol}^{-1} \text{ l s}^{-1}$. The kinetically favored formation of the *endo*-adduct in the second reaction system (reactants **1** and **3**) agrees with the data from the literature; however, we did not observe large difference between the initial rates for the *exo*- and *endo*-adduct formations.

The kinetic measurements at the two temperatures of 300 and 338 K, respectively, also revealed that the estimated activation energies of the formation and decomposition of **7** and the formation of **6** are of the same magnitude, because the rate constants, k_{V}^{f} , k_{V}^{b} , and k_{IV}^{f} increased approximately by a factor of 10. In light of the transition-state theory, we concluded that different magnitudes of the activation entropy, rather than the activation enthalpy, are responsible for the dissimilarity among the rate constants.

A reasonably good fit among dependences among the molar concentrations of single reactants over time can be seen in Figures 2–4. The worst match of the fitted and experimental data for the reactants was accounted

TABLE 4. Calculated Values of Reaction Energies (Hartree–Fock, HF, and Coupled Cluster, CCSD(T) Values; Aug-cc-pVDZ Basis Set; in All Cases MP2/6-31+G(d) Equilibrium Geometries Have Been Used), ΔE , Transition-State Barriers, ΔE^\ddagger , Reaction Gibbs Energies, ΔG , and Activation Gibbs Energies, ΔG^\ddagger , in Vacuo and in Three Solvents for Four Studied Reactions

R1 ^a	R2	P ^b	in vacuo						benzene (C ₆ H ₆)		acetonitrile (CH ₃ CN)		water (H ₂ O)	
			ΔE_{HF}	$\Delta E^\ddagger_{\text{HF}}$	$\Delta E_{\text{CCSD(T)}}$	$\Delta E^\ddagger_{\text{CCSD(T)}}$	ΔG_{vac}	$\Delta G_{\text{vac}}^\ddagger$	ΔG_{benz}	$\Delta G_{\text{benz}}^\ddagger$	ΔG_{acn}	$\Delta G_{\text{acn}}^\ddagger$	ΔG_{w}	$\Delta G_{\text{w}}^\ddagger$
1	2	endo	-31.6	142.2	-86.4	25.2	-14.2	85.6	-12.6	84.5	-24.0	75.6	-31.9	74.1
		exo	-45.0	142.3	-94.4	28.7	-22.3	89.0	-22.0	86.6	-35.5	75.3	-51.7	72.2
1	3	endo	-44.1	145.8	-98.3	26.9	-24.3	87.7	-22.4	87.5	-33.1	80.2	-39.5	80.7
		exo	-57.7	145.5	-106.8	29.0	-33.0	89.8	-32.4	89.4	-43.2	82.0	-57.3	79.2
8	2	endo	-88.6	127.4	-157.6	0.7	-80.0	63.4	-80.9	61.6	-88.9	49.3	-91.7	46.0
		exo	-92.0	136.0	-159.6	10.4	-81.8	72.3	-81.8	70.9	-87.0	60.1	-87.1	54.2
8	3	endo	-99.1	125.9	-168.0	0.9	-88.7	64.1	-88.6	68.2	-95.4	58.2	-94.9	52.5
		exo	-102.3	139.5	-169.3	14.6	-89.8	76.5	-89.2	76.3	-93.8	67.9	-93.4	64.9

^a R1, R2 = reactant 1, 2. ^b P = product. All values are in kJ/mol.

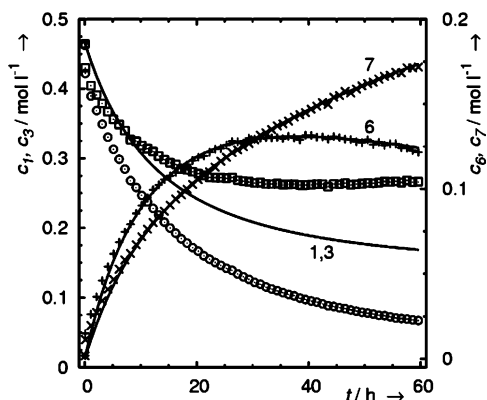


FIGURE 3. Comparison of experimental and predicted responses for reaction of **1** and **3** at 300 K. Experimental points: **1** (○), **3** (◻), **6** (+), **7** (×).

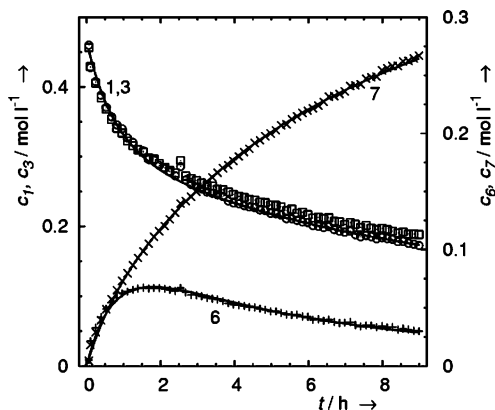


FIGURE 4. Comparison of experimental and predicted responses for reaction of **1** and **3** at 338 K. Experimental points: **1** (○), **3** (◻), **6** (+), **7** (×).

for by a less accurate NMR calibration. This phenomenon especially affected longer runs at a lower temperature (300 K) (see Figure 3) when the mass balance was corrupted by the different molar concentrations of **1** and **3**.

3.2. Quantum Chemical Calculations. To enable us to predict subtle differences in observed kinetics, we used a highly accurate coupled cluster—CCSD(T)—method. We expect to obtain the results with the so-called chemical accuracy of ~ 8 kJ/mol in reaction energies and of ~ 2 kJ/mol in their differences ($\Delta\Delta E$) across the set of the studied reactions.

Four reactions were subject to quantum chemical investigation (furan (**1**) and cyclopentadiene (**8**) as dienes; maleic anhydride (**2**) and maleimide (**3**) as dienophiles), each of them yielding two stereoisomers—*endo* and *exo*. The results, namely gas-phase reaction energies, Gibbs energies, and transition-state barriers, are listed in Table 4. The representative equilibrium geometries of products and transition states are depicted in Figure 5.

Besides the two experimentally studied reactions reported in this paper, the prototypical Diels–Alder cycloadditions with cyclopentadiene (**8**) instead of **1** as a diene on the reactant side were also considered, allowing us to obtain reference values.

The most relevant theoretical data are the values of ΔG and ΔG^\ddagger in an acetonitrile solution, since they can be directly compared to the reported experimental values. The difference in the behavior of dienes **1** and **8** is immediately apparent. Both reactions involving cyclopentadiene (**8**) proceed via a much smaller (by 14–26 kJ/mol) barrier and yield considerably more stable (50–65 kJ/mol) products.⁴⁰ Therefore, the barrier for the backward reaction is higher by 37–40 kJ/mol and, as common knowledge leads us to expect, can be considered the classical examples of kinetically driven processes with a negligible contribution from the reverse reactions.

Furthermore, the barriers for *endo*-adducts are lower by 10–11 kJ/mol and only this adduct is observed under normal conditions. In addition, *endo*-adducts are also thermodynamically more stable, though by only a fairly small amount of 2 kJ/mol.

In contrast, the transition-state barriers for the formation of *endo*/*exo*-adducts are almost identical for both reactions involving furan (**1**) (differing by 0.3 and 1.8 kJ/mol, respectively). The preference for a given stereoisomer is therefore determined by the stability of the product, which is considerably higher for *exo*-adducts (by 12 and 10 kJ/mol, respectively). As the barrier for the backward reaction (compared to **8**) is much lower, this reaction is thermodynamically controlled.

The difference between the behavior of **2** and **3** in both reactions involving **1** is more subtle. The calculated

(39) Zhulin, V. M.; Bogdanov, V. S.; Keltseva, M. V.; Kabotyanskaya, E. B.; Koreshov, Y. D. *Bull. Acad. Sci. USSR D. Chem. Sci.* **1989**, *11*, 2510.

(40) The comparison of energetical values is written as the interval ($x_{\min} - x_{\max}$), where x_{\min} is the minimum value from the set of compared reactions and x_{\max} is the maximum value.

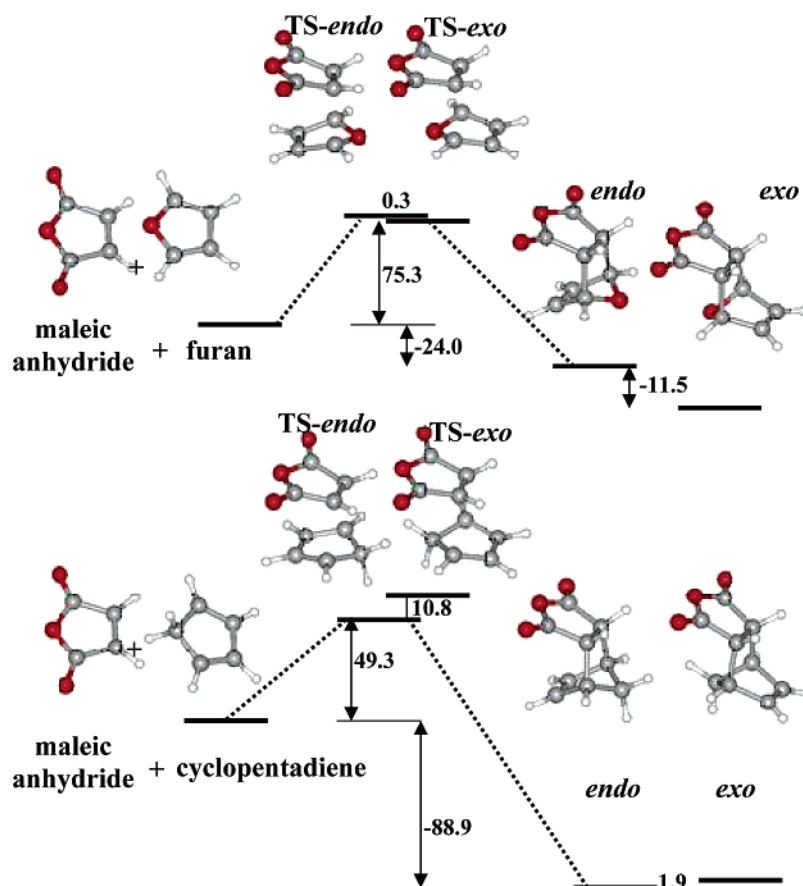


FIGURE 5. Free energy profiles and the MP2/6-31+G(d)-optimized structures of *endo/exo* transition states and products for (1 + 2) and (8 + 2) reactions. All values are in kJ/mol and correspond to the theoretical values for the reaction in acetonitrile solution (see Table 4 for details).

values of $\Delta\Delta G_{\text{endo-exo}} = 12$ and 10 kJ/mol in favor of the *exo*-adduct in reactions (1 + 2) and (1 + 3), respectively, and a slightly higher barrier (2 kJ/mol) for the *endo* reaction channel (compared to *exo*) in the latter reaction (1 + 3) indicate that the formation of *exo*-adduct is preferred in the former reaction (1 + 2). Furthermore, the experimentally measured slower initial formation of (1 + 3) adducts correlates well with the calculated higher reaction barriers (by 5–6 kJ/mol) of both *endo* and *exo* forward reactions (compared to (1 + 2)).

Using the data in Tables 1–3, the above arguments can be formulated quantitatively. The ratios of rate constants between *endo/exo* channels for a specific reaction can be related to the differences among the activation-free energies ($RT\ln(k_{\text{exo}}/k_{\text{endo}}) = \Delta\Delta G_{\text{endo-exo}}$). Thus, for reaction (1 + 2), the experimental $\Delta\Delta G_{\text{endo-exo}}$ value is 1.5 kJ/mol in favor of the *exo* channel, whereas theory predicts 0.3 kJ/mol (Table 4). For reaction (1 + 3), the $\Delta\Delta G_{\text{endo-exo}}$ (exp) = 0.6–0.8 kJ/mol in favor of the *endo* channel, which agrees nicely with the calculated 1.8 kJ/mol. Finally, for retro-(1 + 3) reaction, we obtain $\Delta\Delta G_{\text{endo-exo}}$ (exp) = 7–12 kJ/mol to compare with $\Delta\Delta G_{\text{endo-exo}}$ (theor) = 11.9 kJ/mol. Thus, one can see that the calculated data are within ~ 1 kJ/mol of the experimental results, which gives us the confidence to draw the quantitative conclusions from the calculated data.

When water and benzene are used as the solvents rather than acetonitrile, the calculations predict some notable differences. While the trends for 8 are more or

less identical (the only important difference being the equal thermodynamic stability of *exo*- and *endo*-adducts in benzene solution), the reactivity of diene 1 differs. In benzene, the two reactions (1 + 2) and (1 + 3) should yield identical ratios between the *exo/endo*-adducts (normalized by the total reaction turnover), since $\Delta\Delta G_{\text{endo-exo}}$ are 9.4 and 10.0 kJ/mol, respectively. On the other hand, water (or a strongly polar medium) favors the formation of the *exo*-adduct for both reactions to a much greater extent than do acetonitrile and benzene.

Recently, there have been discussions about the relevance of the concept of secondary orbital interactions (SOI) for the stereoselectivity of Diels–Alder reactions.^{15,22,16} In particular, García et al.¹⁵ presented a thorough discussion of the subject and concluded that alternative explanations (steric and electrostatic interactions, solvent effects, and hydrogen bonding) can explain the origins of *endo/exo* selectivity for many prototypical DA cycloadditions. Nevertheless, our data allow us to add a few arguments to the discussion about SOI and the observed differences in the behavior of furan and cyclopentadiene.

First, the propensity of furan to undergo retro-Diels–Alder reaction can be explained. As has been discussed, furan adducts are less stable than cyclopentadiene ones (with 2 and 3 as the dienophiles) by approximately 50 kJ/mol considering free energy values in acetonitrile solution. Even greater value for enthalpies or free energies in vacuo (57–71 kJ/mol) were calculated favoring

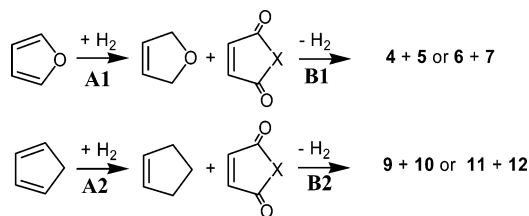


FIGURE 6. Thermodynamic cycle used to explain the higher stability of cyclopentadiene adducts. The cycloaddition is divided into two reactions, i.e., hydrogenation of the reactant (diene) and the closure of the ring with concomitant elimination of hydrogen molecules.

retro-DA reaction channel. A fairly simple explanation of the phenomenon can be traced to the aromatic (de-)stabilization of the furan ring (delocalization of π -electrons), which occurs when moving from a reactant to an adduct. In an adduct, the electronic structure of furan moiety (2,5-dihydrofuran-2,5-diyl residue) is similar to 2,5-dihydrofuran (nonaromatic system), whereas in the analogical cyclopentadiene (nonaromatic system) to cyclopentene route, only one π -bond is lost, and no aromatic destabilization occurs. To quantify the above argument, we have calculated the reaction energies of two hydrogenation reactions as depicted in Figure 6.

The total reaction free energy of the overall DA cycloaddition (e.g., **1** + **2**) can be decomposed as $\Delta E_{\text{tot}} = \Delta E_1 + \Delta E_2$, where ΔE_1 corresponds to the first hydrogenation step and ΔE_2 to the reaction of the 2,5-dihydrofuran (cyclopentene) with **2**, accompanied with a loss of hydrogen atoms. Since the energy difference for the overall reaction is ~ 70 kJ/mol (furan vs cyclopentadiene adducts), it must be also expressed in either ΔE_1 or ΔE_2 (or both). And indeed, the calculated difference—at the DFT(B3LYP)/6-311++G(2d,p) level—in the reaction energies for A1 and A2 (see Figure 6) is 72 kJ/mol (in favor of A2, i.e., the stability of cyclopentene or equivalently, in favor of reverse A1, i.e., stability of furan as the reactant). This value is almost identical as the difference in the stability of furan and cyclopentadiene adducts. Therefore, ΔE_2 must be almost equal for both B1 and B2 reactions (cycloadditions). In summary, the loss of aromaticity (delocalization of π -electrons) in furan destabilizes its adducts, opens a channel for reverse reaction, and causes the reaction to be thermodynamically controlled. It is not necessary to invoke the SOI concept (which is based on transition-state structures, i.e., kinetically controlled reactions) in order to describe the origin of its irregular behavior.

Second, we can add quantitative arguments to the discussion about the origins of *endo/exo* selectivity, based on the energy partitioning scheme that is similar that the above one (García et al.). We add one more contribution—correlation energy—since we consider the SOI concept to be based on a simple orbital picture, i.e., the concept that is meaningful for either single configuration Hartree–Fock (HF) or multireference CASSCF wave functions. Rather elaborate efforts would be necessary to interpret the reasons for the observed *endo/exo* selectivities in terms of highly correlated wave functions (e.g., natural orbital occupation numbers) or Kohn–Sham orbitals in DFT methods.⁴¹

A. Correlation Energy. Comparing ΔE_{HF} , and $\Delta E_{\text{CCSD(T)}}$ values in Table 4, it is apparent that the inclusion of correlation energy changes the values of reaction energies by 49–69 kJ/mol and of the reaction barriers by 114–125 kJ/mol (energy has been severely overestimated by the HF method, in accordance with the findings for the simplest DA reactions).⁴² Since there is not a unique and unambiguous definition of molecular orbitals in correlated wave function techniques, the deviations would seem to prohibit using SOI to explain the stereoselectivity of DA reactions, since even $\Delta \Delta E^+$ values for four reactions vary by up to 10 kJ/mol. The only encouraging finding is that the $\Delta \Delta E$ and $\Delta \Delta E^+$ values for two channels (*endo/exo*) of a particular reaction do not deviate by more than 3 kJ/mol for transition-state barriers and 5 kJ/mol for reaction energies, when comparing HF and CCSD(T) values. Still, this deviation constitutes an order of magnitude in the rate and equilibrium constants.

B. Solvation Effects. As discussed above, the various solvents influence the course of DA reactions. First, the overall stabilization of products and transition states does occur (comparing ΔG_{vac} and $\Delta G_{\text{solvent}}$ values in Table 4). A close inspection of differences between the reaction energies ($\Delta E_{\text{CCSD(T)}}$, $\Delta E^+_{\text{CCSD(T)}}$) and free energies in three solvents reveals variations of up to 10 kJ/mol in the stability of the products and up to 5 kJ/mol in transition-state barriers, which is 1 order of magnitude in rate constants for *endo/exo* channels. Therefore, solvent effects significantly influence the selectivity of Diels–Alder reactions.

C. Electrostatic Forces. It has been noted by García et al.¹⁵ that electrostatic forces, namely repulsion and attraction between the nonbonded atoms during the formation of an adduct, can explain the exceptional behavior of furan. In principle, these forces can be obtained using the molecular mechanics force field. To this end, we have carried out the electrostatic potential fitting (ESP) analysis, i.e., assigning point charges to atoms in molecules using the Merz–Kollman–Singh scheme.⁴³ This procedure is used in the AMBER force field. The calculation of electrostatic energy between nonbonded atoms should give a crude estimate of the stabilization/destabilization of studied DA adducts and transition states. The results of the analysis are summarized in Table S1 (Supporting Information). Only one trend is reproduced consistently and satisfactorily, namely, the higher stability of cyclopentadiene *endo*-adducts with respect to furan *endo*-adducts. Otherwise, the values of electrostatic energy do not correlate systematically with the energy values acquired from quantum chemical calculations, or the origins of DA selectivity *cannot* be explained by simple (MM-like) electrostatics.

In summary, we have attempted to demonstrate that the selectivity of the Diels–Alder reaction is governed by the interplay among various factors, many of which are outside the scope that can be addressed by SOI (e.g.,

(41) Koch, W.; Holthausen, M. *A Chemist's Guide to Density Functional Theory*; Wiley-VCH: Weinheim, 2001.

(42) Wiest, O. in *Encyclopedia of Computational Chemistry*; Schleyer, P. v. R., Ed.; Wiley: Chichester, 1998; p 3104.

(43) (a) Besler, B. H.; Merz, K. M., Jr.; Kollman, P. A. *J. Comput. Chem.* **1990**, *11*, 431. (b) Singh, U. C.; Kollman, P. A. *J. Comput. Chem.* **1984**, *5*, 129.

correlation energy, solvation effects). The concept is not necessarily erroneous, but its usefulness is limited for predicting differences on the order of 5–10 kJ/mol (e.g., the difference in the course of **1** + **2** and **1** + **3** reactions studied for this paper).

4. Conclusions

Clear and consistent experimental data elucidating the kinetics of two Diels–Alder [4 + 2] pericyclic reactions of diene **1** with dienophiles **2** and **3** were presented in this study. Using ^1H NMR data obtained in acetonitrile- d_3 , we showed that at the onset of the reaction, the *endo*-stereoselectivity was not as high as had been reported¹⁹ and the obtained kinetic constants show only a small preference (1.40) for reaction **1** + **3** or even a slight *exo* preference (0.57) for reaction **1** + **2**. We showed that the isomeric composition of products must lie within the varying levels of thermodynamic stability of the formed adducts. The *endo*-adduct **4** decomposes at a very high rate ($1.38 \times 10^{-4} \text{ mol}^{-1} \text{ l s}^{-1}$), while the corresponding *exo*-adduct is much more stable (see Table 1). The dichotomy of kinetic versus thermodynamic control can be clearly seen in the reaction of **1** with **3**. Increasing the reaction temperature by 38 K increases the rate constants of formation of *endo/exo* isomers about 10 times, whereas the retro-Diels–Alder reaction of *endo*-adduct **6** increased 50 times and the reverse reaction of **7**, only 10 times.

The experimental data are well supported by CCSD(T) ab initio calculations of the reactant, product, and transition-state structures and by the reaction energies, free

energies, and solvation energies of the studied species in acetonitrile, water, and benzene solutions.

This work provides a firm experimental and theoretical basis for the remarks of Cooley and Williams⁴⁴ on the kinetic versus thermodynamic control of DA reactions. It is encouraging that the presented theoretical data agree quantitatively with the experimental observations, such as the predicted height of the transition-state barrier for (**1** + **3**) compared to the (**1** + **2**) reaction (5–6 kJ/mol in favor of the latter), which is in accordance with the smaller reaction rate of the former one. Finally, we offer several arguments explaining qualitatively some of the computed values and demonstrate that the SOI concept is of limited use in explaining the observed trends in the title reactions.

Acknowledgment. This work was supported by projects LC512 (MSMT CR) and Z4 055 0506. We thank to J. Doubský for preparing adduct **7**, B. Schneider for help with NMR experiments, and Ms. E. Wheeler for proofreading of the manuscript.

Supporting Information Available: General experimental methods for compound **7**, calculated geometries, and values of electrostatic energies for compounds **4**–**7** and **9**–**12**. This material is available free of charge via the Internet at <http://pubs.acs.org>.

JO050759Z

(44) Cooley, J. H.; Williams, R. V. *J. Chem. Educ.* **1997**, *74*, 582.